Article

Highly Selective Adsorption on SiSe Monolayer and Effect of Strain Engineering: A DFT Study

Quan Zhou [1], Lian Liu [1], Qipeng Liu [1], Zeping Wang [1], Chenshan Gao [1], Yufei Liu [1,2]
and Huaiyu Ye [3,4,*]

[1] Key Laboratory of Optoelectronic Technology & Systems, Education Ministry of China, College of Optoelectronic Engineering, Chongqing University, Chongqing 400044, China
[2] Centre for Intelligent Sensing Technology, College of Optoelectronic Engineering, Chongqing University, Chongqing 400044, China
[3] School of Microelectronics, Southern University of Science and Technology, Shenzhen 518055, China
[4] Shenzhen Institute of Wide-Bandgap Semiconductors, No.1088, Xueyuan Rd., Xili, Nanshan District, Shenzhen 518055, Guangdong, China
[*] Correspondence: h.ye@tudelft.nl

Abstract: The adsorption types of ten kinds of gas molecules (O_2, NH_3, SO_2, CH_4, NO, H_2S, H_2, CO, CO_2, and NO_2) on the surface of SiSe monolayer are analyzed by the density-functional theory (DFT) calculation based on adsorption energy, charge density difference (CDD), electron localization function (ELF), and band structure. It shows high selective adsorption on SiSe monolayer that some gas molecules like SO_2, NO, and NO_2 are chemically adsorbed, while the NH_3 molecule is physically adsorbed, the rest of the molecules are weakly adsorbed. Moreover, stress is applied to the SiSe monolayer to improve the adsorption strength of NH_3. It has a tendency of increment with the increase of compressive stress. The strongest physical adsorption energy (-0.426 eV) is obtained when 2% compressive stress is added to the substrate in zigzag direction. The simple desorption is realized by decreasing the stress. Furthermore, based on the similar adsorption energy between SO_2 and NH_3 molecules, the co-adsorption of these two gases are studied. The results show that SO_2 will promote the detection of NH_3 in the case of SO_2-NH_3/SiSe configuration. Therefore, SiSe monolayer is a good candidate for NH_3 sensing with strain engineering.

Keywords: SiSe monolayer; sensor; DFT; adsorption; stress

1. Introduction

As people care more about physical health and living environment, gas dectection [1,2], especially for the harmful gases has attracted much attention [3–7], such as the monitoring of indoor formaldehyde [8,9] gas content or the leakage of ammonia [10] in chemical plants. The detector can warn in advance when the gas leaks or is excessive. Thus, the gas sensor [11,12] requires sensitive materials which have ability to convert gas information into electrical signals, such as potential or resistance [13].

The principle of gas sensor includes chemical adsorption and physical adsorption. Chemisorption has strong interaction and a slow reaction rate caused by the chemical bond between adsorbent and adsorbate. On the contrary, physical adsorption is weak and faster caused by intermolecular Van der Waals attraction without chemical reaction and is easy to recover. Physisorption and chemisorption are not absolutely isolated from each other and can be changed from one to another. Adsorption properties of sensing materials can be adjusted through a variety of physical or chemical methods [14]. The weak interaction between adsorbate and adsorbent can be enhanced by heating [4], doping [15,16], and even

possibly transformed into chemisorption, while strong adsorption can be weakened under the impact of charge injection [10] and electric field [17]. In addition, original chemical adsorption is converted to physical adsorption [18], which is in favor of gas sensing. However, the above-mentioned modification methods are characterized as instable and complex. Recently, Yu et al. have calculated that chemical adsorption of NH_3 by Ti_2CO_2 substrate is improved by stress [19]. Ma et al. have explained that the moderate adsorption of SO_2 was further enhanced by applying tensile stress [20]. Park et al. prepared the MoS_2 bilayer on substrate by chemical vapor deposition (CVD) and utilized the load test machine of strain gauge presenting different strength [21]. Therefore, stress is a simple, effective, and suitable method for the adjustment of gas adsorption.

For high sensitivity detection, novel two-dimensional (2D) materials are considered to have great potential due to the quantum size effect [22] and exposed active sites. For example, graphene [23–25] or single-layer phosphorene [26–28] has attracted much attention because of high selectivity and sensitivity in adsorption behavior. In particular, the black phosphorus gas sensor has been confirmed by experiments to be a good detector for NO_2 gas molecule [29]. The pleated structure of phosphorene is susceptible to strain [30,31] and its electrical properties can be easily regulated through stress. However, inherent defects of phosphorene and instability in air hinder its further development. Recently, the SiSe monolayer [32,33], with similar structure of phosphorene has shown higher stability than phosphorene. Sa et al. proposed that the good stability of SiSe material is an ideal candidate of building block structure [34]. Yang et al. demonstrated that SiSe monolayers made from non-toxic and earth-abundant elements intrinsically have low thermal conductivities [35]. It is also reported that SiSe can be applied in a battery [36,37] due to large adsorption energies towards single Na and Li atoms, on account of the lower activation energy and rich active sites. These properties may also be expected to be utilized in gas sensor. Especially, an SiSe monolayer with abundant sources in the earth possesses a tunable electronic structure [38] and flexibility under stress, which is conducive to gas adsorption.

Herein, based on the density-functional theory (DFT), adsorption mechanisms and adsorption types of SiSe monolayer with different molecules (O_2, NH_3, SO_2, CH_4, NO, H_2S, H_2, CO, CO_2, and NO_2) are studied. From the perspective of structure and electronic properties, the behavior of NH_3 molecules on the SiSe substrate is physical adsorption with moderate adsorption energy, while SO_2, NO, and NO_2 molecules on SiSe substrate show chemical adsorption with larger adsorption energy. Further, stress is used to adjust the adsorption performance. Results show that the adsorption of NH_3 works best when 2% compressive stress is added to the substrate in zigzag direction, maintaining the maximum physical adsorption characteristics. It is also proved that the NH_3 gas can be desorbed when the stress is removed. By contrast, the SO_2 system exhibits stronger chemical adsorption under compressive stress. Then co-adsorption of SO_2 and NH_3 gas has also been studied due to the interference of each other. We find that the SO_2 molecule promotes the adsorption of NH_3 to some extent, which is advantageous as an NH_3 gas sensor.

2. Materials and Methods

In this work, the DFT theory calculations is conducted by using the CASTEP module and Dmol^3 package of Materials Studio, with generalized gradient approximations (GGA) [39] to Perdew-Burke-Ernzerhof (PBE) [40] functional for the exchange-correlation term [41]. In addition, the Grimme method is used as a dispersion correction to describe the interlayer Van der Waals interaction [42]. The systems are constructed with $3 \times 3 \times 1$ SiSe supercell as substrate and gas molecules are placed above the monolayer. Due to the difference between polar and non-polar molecules, non-spin polarization method is used in (CO_2, NH_3, CO, H_2S, CH_4, SO_2, and H_2O)/SiSe adsorption systems, and spin polarization calculation is used in (NO_2, O_2, and NO)/SiSe adsorption systems. The vacuum layer is set to 20 Å in the (0 0 1) lattice plane to reduce periodic interaction between the layers in the vertical direction. In our simulation, the energy cutoff of the plane wave base is set as 500 eV. The brillouin zone integration is used for geometric optimization and electronic performance calculation on $16 \times 16 \times 1$ grid. All atomic coordinates and lattice constants gradually

relax until a force converges within 0.01 eV Å^{-1} per atom and the tolerance of energy is less than 1.0 e^{-5} eV per atom. The adsorption energy is defined in the following equation [43]:

$$E_a = E_{SiSe+gas} - E_{SiSe} - E_{gas}, \tag{1}$$

where $E_{SiSe+gas}$, E_{SiSe}, and E_{gas} represent the total energy adsorbed by the gas on the SiSe substrate, the SiSe monolayer, and the gas molecules, respectively. Here we mainly focus on absolute value, the greater the absolute value of the adsorption energy, the stronger the interaction between the SiSe monolayer and the gas molecules.

The charge density difference (CDD) map is described to see the charge distribution of gas molecules with the substrate visually and qualitatively. The CDD is based on following definition with charge analysis [44]:

$$\rho = \rho_{gas+SiSe} - \rho_{SiSe} - \rho_{gas}, \tag{2}$$

In this formula, $\rho_{SiSe+gas}$, ρ_{SiSe}, and ρ_{gas} represent the total charge density of the gas molecule/SiSe system, the original SiSe monolayer, and the isolated gas molecules. During the analysis, we need to be aware that each component should be in the same position in the adsorption structure.

Electron localization function (ELF) represents the electron location function and depicts the localized distribution characteristics of electrons. By definition, the value of ELF ranges from 0 to 1, marked with blue and red in the map, respectively. When the value is close to 1, this means the electrons of the atoms are highly localized and bonded together.

3. Results and Discussion

3.1. Adsorption on SiSe Monolayer

It begins with the geometry optimization of unit cell of SiSe. Then $3 \times 3 \times 1$ surface cell is constructed, including 9 Si atoms and 9 Se atoms in the surface cell. After full relaxation, the lattice constant of the armchair direction is 3.650 Å (marked "a" in Figure 1), and the lattice constant of the zigzag direction is 4.647 Å (marked "b" in Figure 1) [38], which is similar to the structure of black phosphorus (4.57 Å and 3.51 Å respectively) [45]. The covalent bond length between Si-Se is tested to be 2.495 Å in horizontal direction (marked "$l_{H(Se-Si)}$" in Figure 1) and 2.467 Å in vertical direction (marked "$l_{V(Se-Si)}$" in Figure 1), which is consistent with previous values [36]. Then, in analyzing the optimal adsorption position displayed in Figure 1, four different adsorption positions are considered, including the "A" position (right above Si-Se bond), the "B" position (on the top of the Si atom), "C" position (right above the center of the honeycomb area), and the "D" position (on the top of the Se atom). The different molecular orientations are also considered in Figure S1. All calculations and analyses are based on systems that the gas molecules at 3 Å away from four sites [43]. After the four configurations converged, we select one configuration with the largest absolute value of the adsorption energy as the object of the next calculation, which is listed in Figure S2. Similarly, other adsorption systems are calculated in the same way. The optimized site of each adsorption system is shown in Table 1.

To discuss the difference in adsorption of different gases on SiSe monolayer, the adsorption energy and distance are calculated (seeTable 1). After full relaxation, NO and NO_2 configurations manifest the biggest adsorption energy (|−0.734| eV and |−0.735| eV, respectively) with the shortest adsorption distance (1.835 Å and 1.995 Å) among all the systems. In addition, the Se-Si bond enlarges to 2.608 Å in the vertical direction and 2.409 Å in the horizon direction, which are attributed to the strong interaction with the substrate. By contrast, compared with other gas configurations, CO, O_2, CO_2, and H_2S molecules have repulsive interaction with the substrate, judged from their increased adsorption distance than the initial state. Other gas molecules like H_2O are preliminarily considered as weak interaction with the substrate based on low adsorption energy. Specially, NH_3 and SO_2 configurations have moderate adsorption energy values (|−0.414| eV and |−0.489| eV, respectively). The

distance between adsorbates and adsorbents is reduced to 2.471 Å and 2.733 Å, respectively. The Si-Se bond is slightly distorted, whose adsorption mechanisms are obscure and need further analysis.
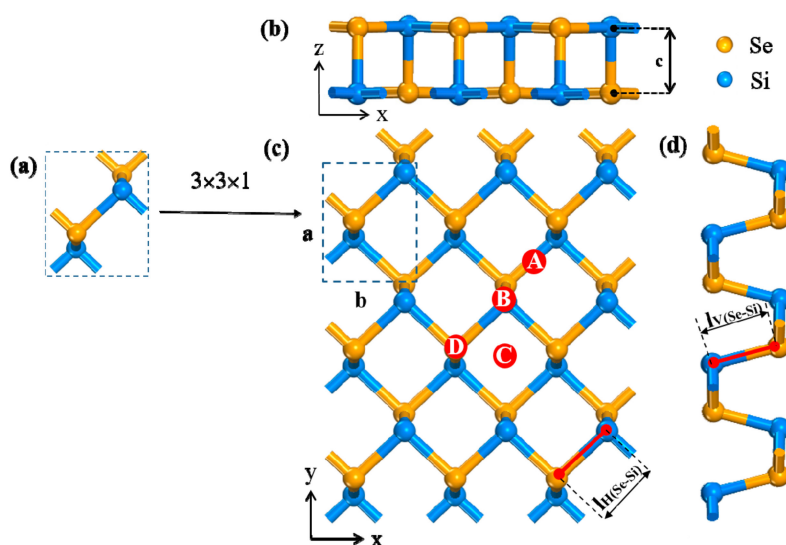

Figure 1. (**a**) Unit cell, (**b**) front, (**c**) top, and (**d**) side view of (0 0 1) lattice plane of substrate. The four sites "**A**", "**B**", "**C**", and "**D**" are respectively labeled in the top view. "x", "y", and "z" are the lattice directions. The marked "**a**" and "**b**" represent the lattice constant of unit cell.

Table 1. The optimal adsorption position, adsorption energy (E_{ad}), closest distance (d), charge transfer (ΔQ), and the length of Si-Se bond. The distance is defined as the nearest two atomic center distances between the gas molecules and the SiSe monolayer. ΔQ is from Hirshfled/Mulliken population analysis, a negative value of ΔQ represents that electrons are transferred from the SiSe monolayer to the gas molecule. The two values of SiSe bond represent the horizontal direction ($l_{H(Se-Si)}$)/vertical direction ($l_{V(Se-Si)}$).

Configuration	Site	E_{ad}(eV)	d (Å)	ΔQ (e)	Si-Se(Å)
CO	C	−0.071	3.577	0.002/0.008	2.497/2.462
O_2	B	−0.098	3.067	−0.032/−0.037	2.492/2.467
CO_2	D	−0.132	3.424	−0.016/-0.016	2.495/2.469
CH_4	A	−0.133	3.084	−0.066/0.022	2.497/2.463
H_2S	A	−0.203	3.405	0.068/0.080	2.503/2.497
H_2O	C	−0.237	2.805	−0.097/0.032	2.487/2.463
NH_3	B	−0.414	2.471	0.153/0.178	2.503/2.658
SO_2	A	−0.489	2.686	−0.238/−0.197	2.448/2.441
NO	B	−0.734	1.835	−0.220/−0.355	2.417/2.528
NO_2	B	−0.735	1.995	−0.285/−0.386	2.409/2.608

In order to clarify the interaction between molecules and SiSe monolayer, the CDD map and ΔQ are calculated to see the charge distribution of gas molecules with the substrate qualitatively and quantitatively. We have listed some typical CDD maps that reflect the different degrees of interaction between the substrate and the gas molecules. The incremental tendency of adsorption strength is displayed from Figure 2a to Figure 2f. In Figure 2a, the CO configuration has substantially no accumulation and consumption of charge at the interface with a little ΔQ, and the same situation happens in the CO_2 configuration (see Figure S3). In other systems, such as O_2, CH_4 etc., the substrate and the gas have a weaker charge rearrangement as shown in Figure 2b, which manifests the stronger interaction with the substrate than CO configuration. Yet the interaction is still much smaller. In Figure 2c,d, the range of charge redistribution of NH_3 configuration and SO_2 configuration are distinctly expanded. The charge is more severely depleted on the NH_3 molecule, while the accumulation on the SO_2 molecule is more serious, indicating that there is a strong interaction between the gas molecules and the substrate. Correspondingly, ΔQ of these two systems is an order of magnitude larger than other six

weak systems mentioned above. In the Figure 2e,f, the interaction between NO and NO_2 structures still maintain the strongest position—the maximum range of charge rearrangement and a significant charge accumulation consumption. It shows, apparently, the loss of charge locates on the substrate, while the increase in charge is concentrated on the gas molecules, where charge is transferred from the gas molecule to the SiSe monolayer. In addition, the stronger interaction matches bigger charge transfer value (|-0.258| e) in NO_2 configuration. It is worth noting that charge transfer of SO_2 molecule shows an abnormal change (|-0.238| e), increasing sharply compared to the NH_3 molecule, even bigger than the NO molecule (|-0.220| e), which implies a different adsorption type from NH_3 configuration.
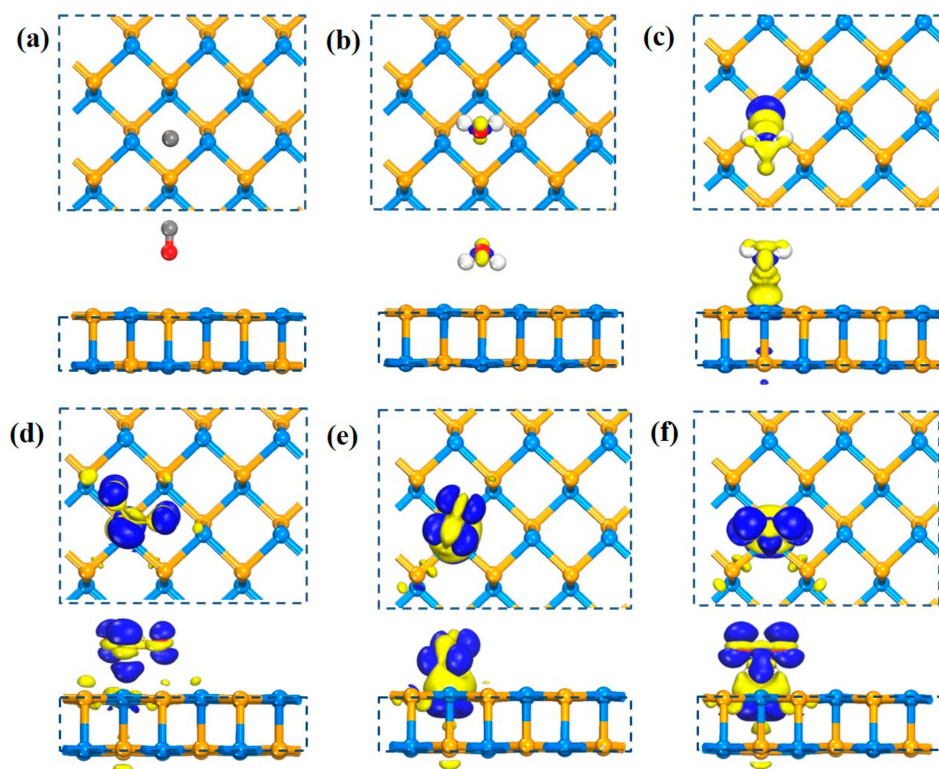

Figure 2. Front and top charge distribution view of charge density difference (CDD) maps, in turn are (**a**) CO, (**b**) H_2O, (**c**) NH_3, (**d**) SO_2, (**e**) NO, (**f**) NO_2 configurations. The yellow part indicates charge loss, and the blue part indicates charge accumulation. The isosurface is set as $0.01e/\text{Å}^3$.

Associated with ELF map in Figure 3a, it is clear to notice that the value of ELF between CO and SiSe substrate is close to 0. There are hardly any electrons between CO molecule and SiSe substrate, which means no electron sharing and no covalent bonds exist in these two components. The same situation also occurs in systems like CH_4, H_2O, H_2S, and O_2 (see Figure S4), which shows that these gas configurations are all physically adsorbed. In Figure 3b, the value of ELF in the border of NH_3 and SiSe monolayer is nearly 0.5, revealing that most electrons are still highly concentrated on the gas molecules and substrate, very little are delocalized in edge of junction. That is to say there exist very few electrons between NH_3 and SiSe monolayer and it is not sufficient to form chemical bonds. On the contrary, it is distinct to see that electron densities of S and Si atoms are connected together and electrons are highly located between them in Figure 3c. It is highly possible to form S-Si covalent bond in the system. In the case of NO_2 system in Figure 3d, the serious orbital overlaps between N atoms and Si atoms displays that they are bonded together, which reflects the chemical adsorption of NO and NO_2 again.

To further confirm the adsorption type, the DOS and PDOS (total and partial densities of states) are calculated.Figure 4a shows plainly that DOS of pristine SiSe substrate is almost changeless near Fermi level before and after the NH_3 is adsorbed on it. The big difference appears at around −5 eV in the valence band far away from Fermi level. In PDOS, it is obvious to find that there is no orbital overlap between NH_3 molecule and SiSe monolayer near CBM (Conduction Band Minimum) or VBM

(Valence Band Maximum). Hence physical adsorption occurs in NH_3 and SiSe monolayer. In next Figure 4b, the DOS of SiSe is slightly offset after SO_2 is adsorbed on SiSe near Fermi level from -2 eV to -3 eV, and the peaks of orbitals between S atom and Si atom are overlapped at the energy of -1 eV in the valence band and 1 eV in the conduction band. From Figure 4c,d, between −8 eV to 4 eV, the DOS of pristine SiSe monolayer is different from the adsorbed systems. The original electrical properties are destroyed when the NO_2 is adsorbed on substrate. The chemical bond is formed with the more serious orbitals' hybridization, combined with the above analysis.
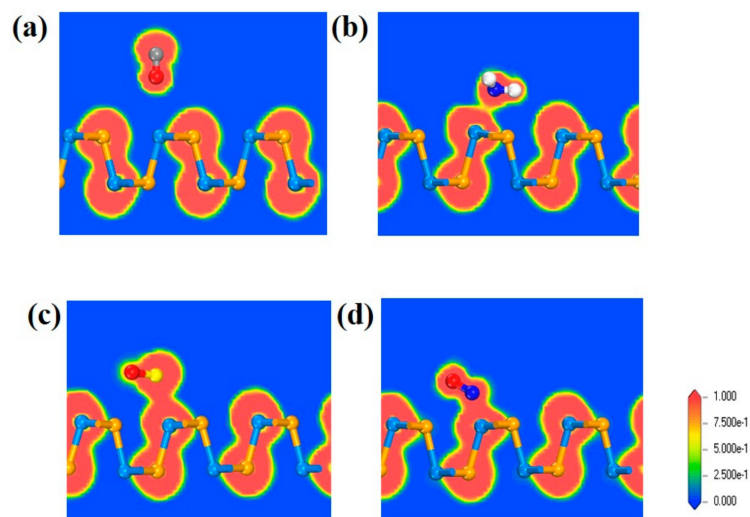
Figure 3. The distribution of electron localization maps of (**a**) CO, (**b**) NH_3, (**c**) SO_2, and (**d**) NO_2 configurations. The reference column for the electron localization function (ELF) value from 0 to 1 is located on the right side of the figure, representing blue and red, respectively. The slice of the ELF is parallel to the (100) crystal plane.
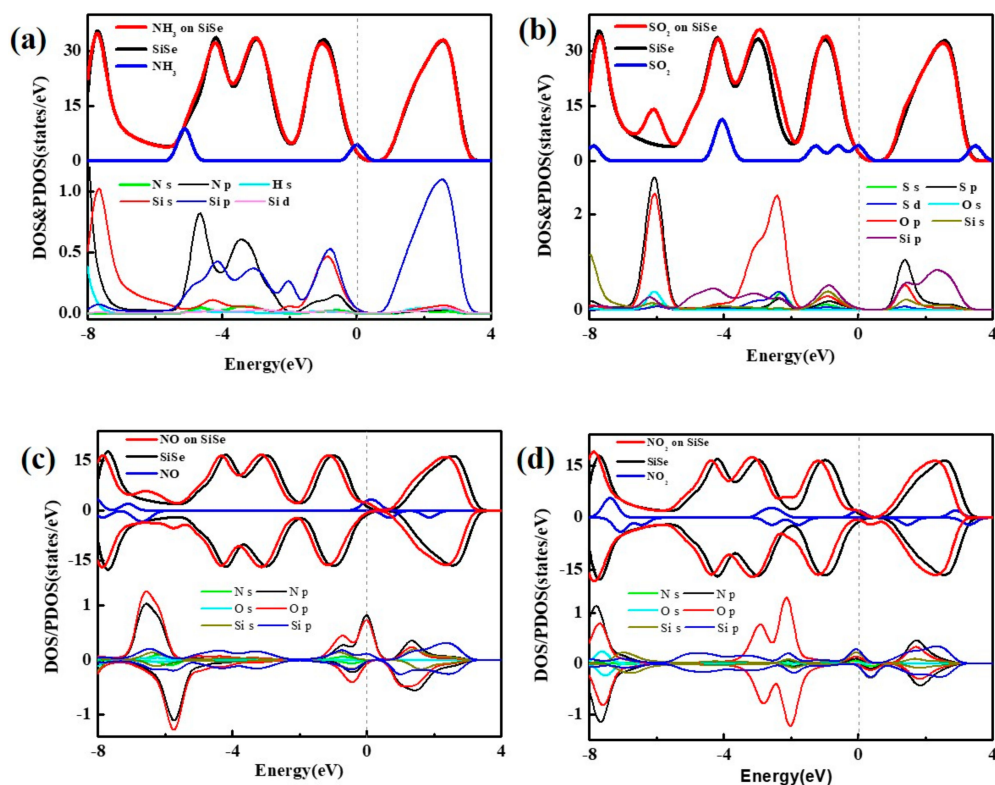

Figure 4. The DOS and PDOS maps of (**a**) NH_3, (**b**) SO_2, (**c**) NO, and (**d**) NO_2 molecules adsorbed on SiSe monolayer.

In total, the high selectivity is displayed based on above analysis associated with the electronic analysis: the interaction between the NH_3 gases and the SiSe monolayer is the strongest physical adsorption property with moderate adsorption energy (−0.414 eV), which is larger than previous researches [4,19,27], and makes it possible for SiSe monolayer to adsorb NH_3 and easily desorb. SO_2, NO or NO_2 gases on the SiSe monolayer show the chemisorption property. The chemical reaction with substrate makes it difficult to reuse. The rest of the gases have very weak interaction with SiSe monolayer. They are all not suitable as a gas sensor based on the SiSe monolayer.

3.2. Adsorption Mechanism of NH_3 Under Stress

Due to the special corrugated structure of SiSe, the adsorption property with SiSe monolayer under stress is discussed. Stress has been used to effectively regulate the mechanical, electrical, and magnetic properties of semiconductors over the past researches [46–49]. Previous theoretical and experimental studies indicate that the application of in-plane strain can adjust the band gap of SiSe monolayer [38], yet the performance of the SiSe monolayer adsorbing gas after the stress has not been studied. NH_3 needs to be detected as a harmful gas, stress calculations are performed along the X-axis (zigzag direction), Y-axis (armchair direction), and biaxial directions, respectively (shown in Figure 5). The stress is defined as: $\varepsilon = (a − a_0)/a_0$, where "$a_0$" and "$a$" are the lattice parameter of the original cell and strained-cell, respectively [19]. The gas is adsorbed on systems with the substrate stretched or compressed from 0% to 8% (also recorded −8% to 8%), the changes in various indexes after adsorption are observed.
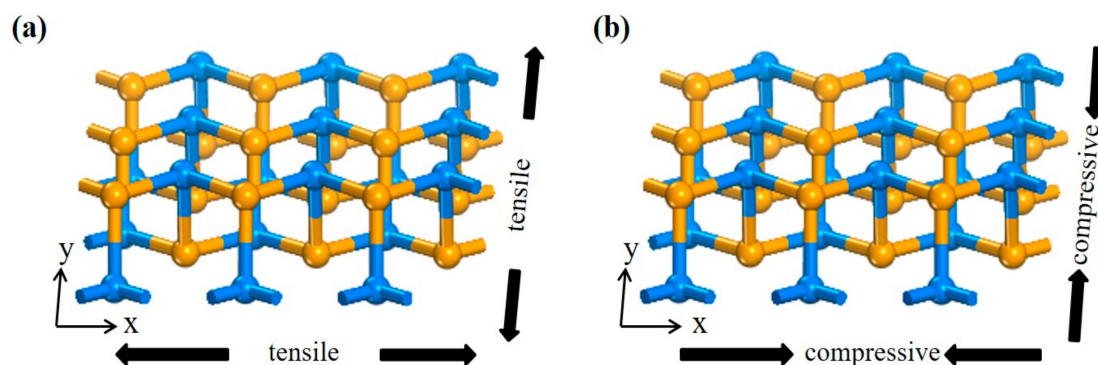

Figure 5. Schematic diagram of SiSe monolayer under in-plane (**a**) compressive (**b**) tensile stress from X-axis, Y-axis, and biaxial direction.

3.2.1. Compressive Direction

First, under the uniaxial X-axis compression, the adsorption energy is gradually increased. When the stress reaches −8%, the adsorption energy increases to a maximum value of |−0.46| eV, which indirectly reflects the enhancement of the interaction between the NH_3 molecule and the substrate. Further, this enhancement may result in the formation of covalent bonds between the NH_3 molecule and the substrate. Therefore, the research on the ELF chart is performed. As present in Figure 6a, the electron local density of the NH_3 molecules does not overlap with the SiSe substrate in ELF slice until the compressive stress reaches to 4%, and it is seen that a covalent bond is likely to be formed, which is in the progressing direction that is unfavorable to the gas sensor. Thus, it shows the best adsorption efficiency when −2% stress is added to the substrate. Similarly, the compressive strain trend in the Y-axis and the biaxial are the same as the compressive strain trend in the X-axis (as shown in Figure 6b). Only the degree of change is different: biaxial > Y-axis > X-axis. When the stress is from −4% to −8%, the rate of change in adsorption energy is sharply increasing and the adsorption energy increases to |−0.78| eV at −8%, which is greater than the adsorption energy of NO_2 system. At this time, observing the ELF diagram, it can be seen that the electron local density range of the N and Si atom are greatly hybridized (see inset of Figure 6b). A strong chemical bond is formed between the

N and the Si atoms. That is to say, chemical adsorption is formed between the substrate and the gas, and the compressive stress enhances the adsorption of the gas.
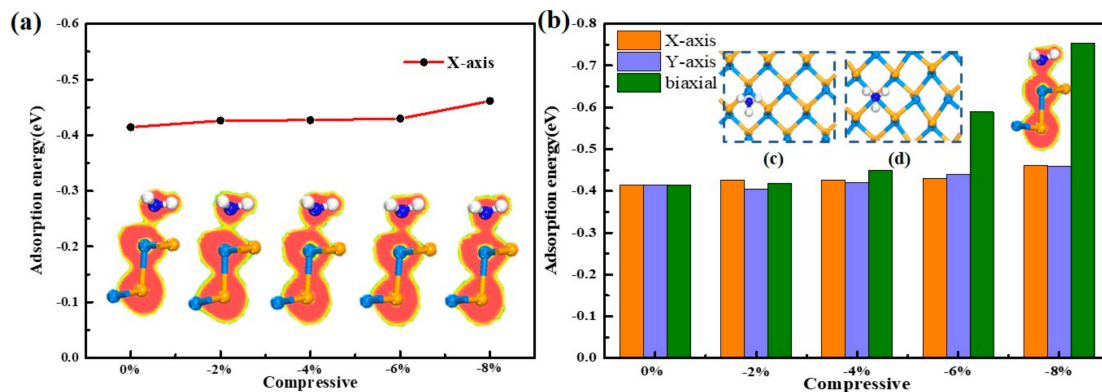
Figure 6. (**a**) The change curves of E_{ad} with compressive strain from 0% to −8% in NH_3/strained-SiSe systems, ELF from left to right represents 0%, −2%, −4%, −6%, and −8% of stress. (**b**) The comparison of adsorption energy with X-axis, Y-axis, and biaxial under compressive strain from 0% to −8% in NH_3/strained-SiSe systems, the data is shown in Table S1. The inset of (**b**) represents the ELF of −8% biaxial of NH_3/SiSe monolayer. The inset is morphology of NH_3 system (**c**) without stress and (**d**) with −8% stress in biaxial direction.

According to the reversibility of physical adsorption, we try to demonstrate the inverse process of the best adsorption position when −2% pressure is applied to SiSe monolayer. The −2% compression system that has completed the adsorption of NH_3 is pulled back again to the original state of 0% stress-free state. After optimization, the adsorption energy, closest distance, ΔQ and the bond of Si-Se are recorded in Table 2. Comparing the pulled back to the 0% system (label as −2% to 0% NH_3/SiSe) with −2% compressive stress-NH_3/SiSe (label as −2% NH_3/SiSe), it is discovered that adsorption energy is reduced to |−0.413| eV, which is very close to |−0.414| eV at 0%. Additionally, the length of the Si-Se bond and ΔQ both recover to the situation of no stress, which shows an reverse process of gas desorption in gas sensor.

Table 2. The adsorption energy (E_{ad}), closest distance (d), Mulliken charge transfer (ΔQ), and the Si-Se bond of horizontal and vertical direction.

Configuration	E_{ad} (eV)	d (Å)	ΔQ (e)	Si-Se(Å)
0% NH_3/SiSe	−0.414	2.471	0.178	2.503/2.658
−2% NH_3/SiSe	−0.426	2.443	0.184	2.482/2.669
−2% to 0% NH_3/SiSe	−0.413	2.454	0.180	2.505/2.661

In the process of applying compressive stress to the substrate, the NH_3 molecule is found to move close to the Si atom in Figure 6c,d. Moreover, the bond length of Si-Se, ΔQ, and adsorption distance of the adsorption process of biaxial stress are carefully observed in Table 3 due to the obvious change among them. Without compression, after the adsorption is stabilized, the length of Si-Se bond are slightly distorted to 2.502 Å in XY plane and 2.658 Å in YZ plane respectively, the NH_3 molecule will run toward the middle of the corrugate with the Si atom attracted to protrude from the substrate level, causing the substrate to be slightly deformed. As the biaxial compression increases, the $l_{H(Se-Si)}$ gradually decreases to 2.436 Å and 2.444 Å. While the $l_{V(Se-Si)}$ gradually increases to 2.701 Å, meanwhile the adsorption distance is gradually reduced to 2.226 Å, representing the strengthen interaction between the substrate and NH_3 molecule. At this time, the NH_3 molecules no longer run to the middle of the corrugate, but is more close to the Si atom without the silicon atoms prominent out of the horizon. This phenomenon can be explained by charge transfer. When there is no pressure, the ΔQ of Si atom (|0.605| e) and Se atom (|−0.618| e) close to the NH_3 molecule is very large. It can be

seen that the NH_3 molecule is not only attracted by the Si atom, but also restricted by the Se atom, so that the NH_3 molecule will run to the middle, making Si-Se length in the vertical direction increases. As the pressure is applied, the ΔQ of the Si atom (|0.672| e) is gradually larger than that of the Se atom (|−0.563| e), so that the attraction of the Si atom is dominant. Thus, the NH_3 molecule is adsorbed towards the Si atom.

Table 3. Mulliken charge transfer (ΔQ) of Si atom closest to the NH_3 molecule and connected Se atom, the nearest distance (d) and the length of Si-Se bond of NH_3 gas molecule adsorbed on SiSe monolayer after biaxial stress from 0% to −8%.

Parameter		0%	−2%	−4%	−6%	−8%
d (Å)		2.471	2.384	2.351	2.273	2.226
ΔQ (e)	Si	0.605	0.600	0.607	0.644	0.672
	Se	−0.618	−0.602	−0.598	−0.578	−0.568
Si-Se Bond(Å)	Horizontal	2.502	2.494	2.472	2.460	2.444
	Vertical	2.658	2.662	2.672	2.679	2.701

3.2.2. Tensile Direction

For NH_3 configuration, the adsorption energy of the system decreases very little as the tensile force increases, which is contrary to the compression. The adsorption energy in the direction of X-axis slightly decreases to |-0.396| e with the stretch increases, and the Y-axis direction decreases to the minimum value of |-0.313| e with the stretch increases to 4%, then conversely increases to |-0.405| e at 8%. It is noticed that the tensile stress in the Y-axis direction is more significant to the system, and the biaxial is the effect of the X-axis and the Y-axis. As the adsorption energy decreases, the effect of gas and substrate becomes weaker. Combined with ELF in Figure 7a, the range of NH_3 molecule under biaxial stretching does not overlap with the SiSe monolayer, indicating no covalent bond is formed, thus the physical adsorption property remains.
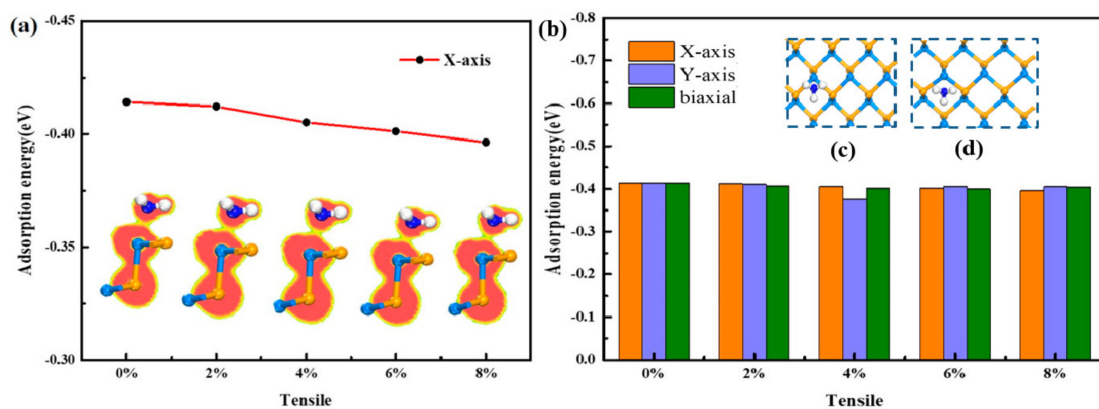
Figure 7. (**a**) The change curves of E_{ad} with tensile strain from 0% to 8% in NH_3/strained-SiSe systems, ELF from left to right represents 0%, 2%, 4%, 6%, and 8% of stress. (**b**) The comparison of adsorption energy with the X-axis, Y-axis, and biaxial under compressive strain from 0% to 8% in NH_3/strained-SiSe systems, the data is shown in Table S1. The inset is morphology of NH_3 system (**c**) without stress and (**d**) with 8% stress in biaxial direction.

When the tensile stress is added to the substrate, the NH_3 molecule moves to the honeycomb instead in Figure 7c,d. The mechanism is studied from the perspective of charge transfer and atomic orbital. First, it can be seen from the ΔQ of the substrate that the Si atom closest to the NH_3 molecule has a large ΔQ and there is a strong interaction with the NH_3 molecule mainly. However, the two Se atoms connected to the Si atom also have large ΔQ (|−0.618| e) that cannot be ignored. In total, the entire NH_3 molecule is simultaneously constrained by these relatively active Se atoms. As the stretching enlarges, the ΔQ of Se atom increases to |−0.627| e at 8% with the enhancement of constraint

action, so that the entire NH_3 molecule is attracted to the middle of the honeycomb. Hence, the Si atom follows the movement of the NH_3 molecule and the Se-Si bond in the vertical direction becomes longer inTable 4.

Table 4. Mulliken charge transfer (ΔQ) of Si atom closest to NH_3 molecule and connected Se atom, the nearest distance (d) and the length of Si-Se bond of NH_3 gas molecule adsorbed on SiSe monolayer after biaxial stress from 0% to 8%.

| Parameter		0%	-2%	-4%	-6%	-8%
d (Å)		2.471	2.503	2.518	2.479	2.465
ΔQ (e)	Si	0.605	0.606	0.607	0.609	0.610
	Se	−0.618	−0.619	−0.626	−0.624	−0.627
Si-Se	Horizontal	2.502	2.527	2.551	2.572	2.596
Bond(Å)	Vertical	2.658	2.649	2.649	2.663	2.679

In the following, the band structure and atomic orbital are discussed to have an in-depth exploration. In the absence of stress displayed in Figure 8a, the system has an indirect band gap of 1.108 eV. Presented in PDOS, the valence band is mainly contributed by the 4p orbital of the Se atom, and the conduction band is mainly contributed by the 3p orbital of the Si atom, which is in accordance with the HUMO (Highest Occupied Molecular Orbital) and LUMO (Lowest Unoccupied Molecular Orbital) in Figure 8c,d. As the tensile force increases, the bandgap of the system increases to 1.295 eV. This may be the reason that the tensile force increases the lattice constant of the substrate and the distance between the atoms becomes larger, thus the energy level of each atom becomes more discrete. The contribution of the P orbital of Se to the conduction band increases, and the effect of Se increases under the tensile force, which is consistent with the previous analysis. At the same time, the contribution of the Si atom to the valence band has also increased, but there is not much increase in Se, and finally the comprehensive influence of the substrate on the adsorption of NH_3 is weakened.
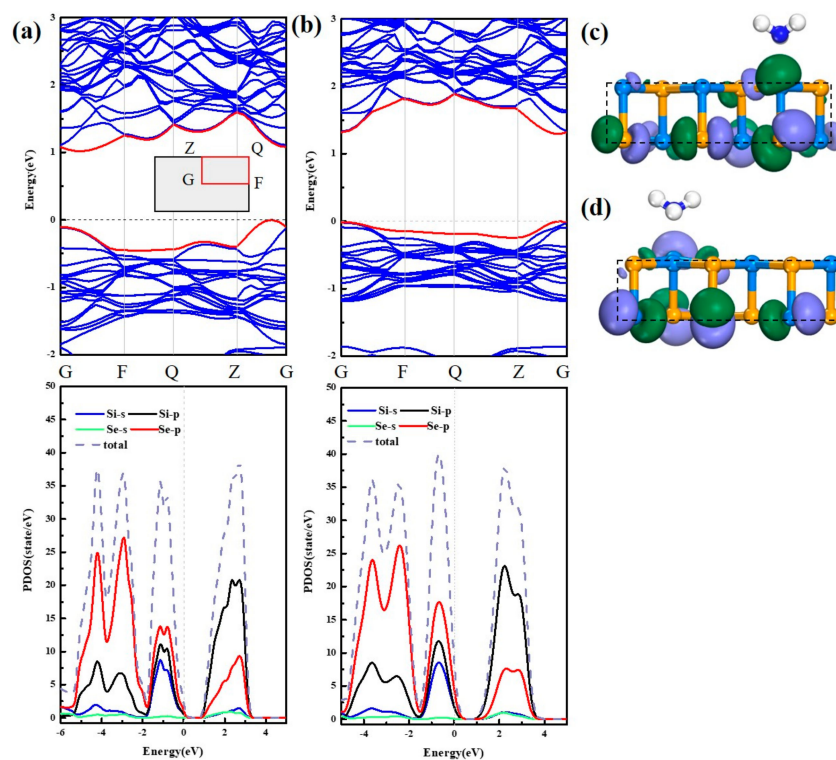
Figure 8. The band structure and PDOS of (**a**) NH_3/ SiSe systems and (**b**) 8% tensile stress-NH_3/SiSe systems, respectively. The inset of (**a**) is the Brillouin Zone path. The Fermi level (the dash line) is set to zero. (**c**) HUMO and (**d**) LUMO.

3.3. Adsorption Mechanism of SO₂ Under Stress

Since the adsorption of SO_2 molecule by the SiSe monolayer is very close to the adsorption of NH_3, it is hoped that the adsorption of SO_2 molecule can be improved by stress, too. Similarly, stress is applied to the substrate from the X-axis, the Y-axis, and the XY-biaxial direction, respectively, and then the SO_2 molecule is adsorbed. The trend of adsorption strength is also the same as NH_3 configuration: the increase of the tensile force causes the decrease of adsorption energy and the ΔQ, while the increase of the pressure causes the increase of adsorption energy and the ΔQ. It has been previously analyzed that the adsorption of SO_2 by the substrate with free-stress is chemisorption, and if the stretching method is employed to reduce the interaction between the substrate and the gas, it is possible to improve the adsorption of SO_2 molecule for gas sensor. Furthermore, the ELF of SO_2 with 8% stress added to the SiSe monolayer is explored. When the tensile stress of X-axis is increasing, the adsorption energy reduces by $|0.073|$ eV and the ΔQ reduces by 0.32 e, showing a declining interaction between the substrate and molecule. However, the region of electron localization between the Si atom and the S atom still overlaps largely in Figure 9a, proving that chemisorption is still present. Although the adsorption energy and the transfer charge reduce more under the tensile stress of Y-axis or biaxial, such as the adsorption energy reaches $|-0.400|$ eV and the ΔQ reaches $|-0.208|$ e under biaxial stretching, but the ELF slice still demonstrates the hybridization between two parts. It is to say that the stress cannot adjust the adsorption of SO_2 to an optimum state.
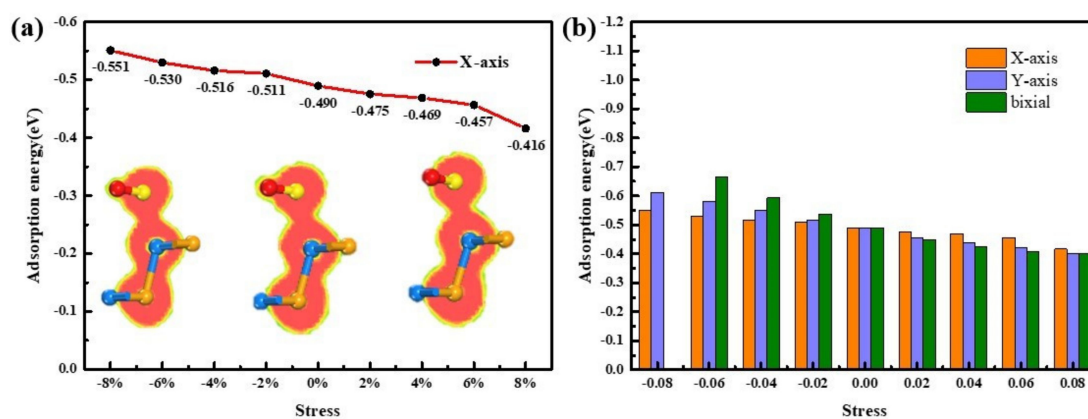
Figure 9. (**a**) The change curves of E_{ad} with tensile strain from −8% to 8% in SO_2/strained-SiSe systems, ELF from left to right represents −8%, 0%, and 8% of stress. (**b**) The comparison of adsorption energy with the X-axis, Y-axis, and biaxial under compressive strain from -8% to 8% in NH_3/strained-SiSe systems.

On account of the small difference in adsorption of NH_3 and SO_2 based on SiSe substrate. It is necessary to discuss the co-adsorption mechanism of SO_2 and NH_3 gas on SiSe monolayer [50]. We consider three possible adsorption manners according to the actual situation: adsorption of SO_2 and NH_3 simultaneously (referred to as SO_2 and NH_3/SiSe), adsorption of SO_2 followed by adsorption of NH_3 (referred as SO_2-NH_3/SiSe) and adsorption of NH_3 followed by adsorption of SO_2 (referred as NH_3-SO_2/SiSe). The results of the calculation are shown in the Table 5 and Table S2. Under these three cases, the substrate exhibits a different strength for gas adsorption. In the case of SO_2 and NH_3/SiSe, the adsorption abilities to the SO_2 molecule and the NH_3 molecule both increase from the data analysis in the table. The ΔQ of NH_3 rises to $|0.241|$ e, which is $|0.063|$ e larger than initial. Meanwhile the ΔQ of SO_2 is 0.046 e larger than original. Both the distances between the molecules and substrate are shortened, with the NH_3 reduced more seriously. It is easy to find that the same situation occurs in NH_3-SO_2/SiSe. Hence, the co-adsorption of NH_3 in the case of SO_2 and NH_3/SiSe and NH_3-SO_2/SiSe shows no sign of decline. Differently, when the SiSe monolayer first adsorbs the SO_2 molecule and then adsorbs the NH_3 molecule, the ΔQ of SO_2 decreases with the adsorption distance of SO_2 increases comparing to the SO_2/SiSe system, indicating that the interaction between the SO_2 molecule and substrate is weakened. The adsorption of NH_3 gas is improved comparing to NH_3/SiSe

system, which may due to the reason that electronegativity of the N atom is greater than S atom. The N and Si atom are more likely to get or lose electrons than the S and Si atom.

Table 5. Adsorption energy (E_{ad}), Mulliken charge transfer (ΔQ), and closest distance (d) of the NH_3 molecule and the SO_2 molecule, respectively in SO_2 and NH_3/SiSe, NH_3-SO_2/SiSe, and SO_2-NH_3/SiSe configurations.

Configuration	E_{ad} (eV)	$\Delta Q_{(NH3)}$(e)	$\Delta Q_{(SO2)}$(e)	$d_{(NH3)}$(Å)	$d_{(SO2)}$(Å)
SO_2 and NH_3/SiSe	−1.161	0.241↑	-0.276↑	2.278↓	2.646↓
NH_3-SO_2/SiSe	−0.752	0.243↑	-0.278↑	2.226↓	2.639↓
SO_2-NH_3/SiSe	−0.465	0.196↑	-0.220↓	2.431↓	2.760↑

4. Conclusions

In conclusion, ten different gases (CO, O_2, CO_2, CH_4, H_2S, H_2O, NH_3, SO_2, NO, NO_2) of adsorption on SiSe monolayer have been studied. From the perspective of adsorption energy, DOS, PDOS, CCD, and ELF, it is found that NH_3 molecule is physical adsorption with moderate adsorption energy of 0.414 eV, which is the most suitable as gas sensor material. On the contrary, the adsorption of SO_2 belongs to chemical adsorption with large adsorption energy (0.490 eV), both NO and NO_2 are equipped with the largest adsorption energy (0.734 eV, 0.735 eV), which can be applied in one-time gas sensor. Further, stress is applied to adjust the adsorption performance of SiSe monolayer to adsorb NH_3 and SO_2 molecules. The results reveal that compressive strain causes the sensitive material sensor to develop toward larger adsorption energy, and the tensile strain changes inversely. Thus, when the stress increases to −2% in the X-axis, the adsorption of NH_3 is enhanced with the adsorption energy increases to |−0.426| eV, which maintains the physical adsorption of NH_3. While for SO_2 molecule, the strength of chemical adsorption based on SiSe monolayer is increased under compressive stress. In addition, due to the small difference of SO_2 and NH_3 molecules, the co-adsorption of these two gases on substrate shows that the adsorption of NH_3 is promoted at three different situations, even the adsorption of SO_2 will be suppressed when the SO_2 is first adsorbed on SiSe monolayer. Therefore, it is expected that the SiSe monolayer is a potential candidate to be applied in NH_3 gas sensors.

References

1. Zhang, J.; Qin, Z.; Zeng, D.; Xie, C. Metal-oxide-semiconductor based gas sensors: Screening, preparation, and integration. *Phys. Chem. Chem. Phys.* **2017**, *19*, 6313–6329. [CrossRef] [PubMed]

2. Joshi, N.; Hayasaka, T.; Liu, Y.; Liu, H.; Oliveira, O.N.; Lin, L. A review on chemiresistive room temperature gas sensors based on metal oxide nanostructures, graphene and 2D transition metal dichalcogenides. *Microchim. Acta* **2018**, *185*, 213. [CrossRef] [PubMed]

3. Wella, S.A.; Aditya, I.D.; Wungu, T.D.K. Density Functional Theory (DFT) Study: Electronic Properties of Silicene under Uniaxial Strain as H2S Gas Sensor. *Key Eng. Mater.* **2016**, *675–676*, 15–18.

4. Ma, S.; Yuan, D.; Wang, Y.; Jiao, Z. Monolayer GeS as a potential candidate for NO2 gas sensor and capturer. *J. Mater. Chem. C* **2018**, *6*, 8082–8091. [CrossRef]

5. Ahn, M.W.; Park, K.S.; Heo, J.H.; Park, J.G.; Kim, D.W.; Choi, K.J.; Lee, J.H.; Hong, S.H. Gas Sensing Properties of Defect-Controlled ZnO-Nanowire Gas Sensor. *Appl. Phys. Lett.* **2008**, *93*, 1502. [CrossRef]

6. Ren, J.; Kong, W.; Ni, J. The Potential Application of BAs for a Gas Sensor for Detecting SO$_2$ Gas Molecule: A DFT Study. *Nanoscale Res. Lett.* **2019**, *14*, 133. [CrossRef]

7. Guo, S.; Lu, Y.; Liu, X.; Zhou, W.; Song, X.; Zhang, S. First-principles study of SO$_2$ sensors based on phosphorene and its isoelectronic counterparts: GeS, GeSe, SnS, SnSe. *Chem. Phys. Lett.* **2017**, *686*, 83–87. [CrossRef]

8. Mirzaei, A.; Leonardi, S.G.; Neri, G. Detection of hazardous volatile organic compounds (VOCs) by metal oxide nanostructures-based gas sensors: A review. *Ceram. Int.* **2016**, *42*, 15119–15141. [CrossRef]

9. Huiru, Y.; Zeping, W.; Huaiyu, Y.; Kai, Z.; Xianping, C.; Guoqi, Z. Promoting sensitivity and selectivity of HCHO sensor based on strained InP$_3$ monolayer: A DFT study. *Appl. Surf. Sci.* **2018**, *459*, 554–561.

10. Bo, X.; Li, Y.C.; Yu, X.F.; Cheng, J.B. MXenes: Reusable materials for NH$_3$ sensor or capturer by controlling the charge injection. *Sens. Actuators B Chem.* **2016**, *235*, 103–109.

11. Yamazoe, N. Toward innovations of gas sensor technology. *Sens. Actuators B Chem.* **2005**, *108*, 2–14. [CrossRef]

12. Choi, J.K.; Hwang, I.S.; Kim, S.J.; Park, J.S.; Park, S.S.; Jeong, U.; Yun, C.K.; Lee, J.H. Design of selective gas sensors using electrospun Pd-doped SnO2 hollow nanofibers. *Sens. Actuators B Chem.* **2010**, *150*, 191–199. [CrossRef]

13. Yang, S.; Jiang, C.; Wei, S. Gas sensing in 2D materials. *Appl. Phys. Rev.* **2017**, *4*, 021304. [CrossRef]

14. Kannan, P.K.; Late, D.J.; Morgan, H.; Rout, C.S. Recent developments in 2D layered inorganic nanomaterials for sensing. *Nanoscale* **2015**, *7*, 13293–13312. [CrossRef] [PubMed]

15. Peyghan, A.A.; Rastegar, S.F.; Hadipour, N.L. DFT study of NH$_3$ adsorption on pristine, Ni- and Si-doped graphynes. *Phys. Lett. A* **2014**, *378*, 2184–2190. [CrossRef]

16. Liang, X.Y.; Ding, N.; Ng, S.P.; Wu, C.M.L. Adsorption of gas molecules on Ga-doped graphene and effect of applied electric field: A DFT study. *Appl. Surf. Sci.* **2017**, *411*, 11–17. [CrossRef]

17. Guo, H.; Zhang, W.; Ning, L.; Zhuo, Z.; Xiao, C.Z.; Wu, X.; Yang, J. CO$_2$ Capture on h-BN Sheet with High Selectivity Controlled by External Electric Field. *J. Phys. Chem. C* **2015**, *119*, 6912–6917. [CrossRef]

18. Zhu, J.; Ha, E.; Zhao, G.; Zhou, Y. Recent advance in MXenes: A promising 2D material for catalysis, sensor and chemical adsorption. *Coord. Chem. Rev.* **2017**, *352*, 306–327. [CrossRef]

19. Yu, X.F.; Li, Y.C.; Cheng, J.B.; Liu, Z.B.; Li, Q.Z.; Li, W.Z.; Yang, X.; Xiao, B. Monolayer Ti$_2$CO$_2$: A Promising Candidate for NH$_3$ Sensor or Capturer with High Sensitivity and Selectivity. *ACS Appl. Mater. Interfaces* **2015**, *7*, 13707–13713. [CrossRef]

20. Ma, S.H.; Yuan, D.; Jiao, Z.Y.; Wang, T.X.; Dai, X. Monolayer Sc$_2$CO$_2$: A Promising Candidate as SO$_2$ Gas Sensor or Capturer. *J. Phys. Chem. C* **2017**, *121*, 24077–24084. [CrossRef]

21. Park, M.; Park, Y.J.; Chen, X.; Park, Y.K.; Kim, M.S.; Ahn, J.H. MoS2-Based Tactile Sensor for Electronic Skin Applications. *Adv. Mater.* **2016**, *28*, 2556–2562. [CrossRef] [PubMed]

22. Wasey, A.H.M.A.; Chakrabarty, S.; Das, G.P. Quantum size effects in layered VX$_2$ (X=S, Se, Te) materials: Manifestation of metal to semimetal or semiconductor transition. *J. Appl. Phys.* **2015**, *117*, 064313. [CrossRef]

23. Docherty, C.J.; Lin, C.T.; Joyce, H.J.; Nicholas, R.J.; Herz, L.M.; Li, L.J.; Johnston, M.B. Extreme sensitivity of graphene photoconductivity to environmental gases. *Nat. Commun.* **2012**, *3*, 1228. [CrossRef] [PubMed]

24. Schedin, F.; Geim, A.K.; Morozov, S.V.; Hill, E.W.; Blake, P.; Katsnelson, M.I.; Novoselov, K.S. Detection of individual gas molecules adsorbed on graphene. *Nat. Mater.* **2007**, *6*, 652–655. [CrossRef] [PubMed]

25. Yuan, W.; Shi, G. Graphene-based gas sensors. *J. Mater. Chem. A* **2013**, *1*, 10078–10091. [CrossRef]

26. Cui, S.; Pu, H.; Wells, S.A.; Wen, Z.; Mao, S.; Chang, J.; Hersam, M.C.; Chen, J. Ultrahigh sensitivity and layer-dependent sensing performance of phosphorene-based gas sensors. *Nat. Commun.* **2015**, *6*, 8632. [CrossRef]

27. Kou, L.; Frauenheim, T.; Chen, C. Phosphorene as a Superior Gas Sensor: Selective Adsorption and Distinct I-V Response. *J. Phys. Chem. Lett.* **2014**, *5*, 2675–2681. [CrossRef]

28. Chen, P.F.; Li, N.; Chen, X.Z.; Ong, W.J.; Zhao, X.J. The rising star of 2D black phosphorus beyond graphene: Synthesis, properties and electronic applications. *2D Mater.* **2018**, *5*, 21. [CrossRef]

29. Abbas, A.N.; Liu, B.; Chen, L.; Ma, Y.; Cong, S.; Aroonyadet, N.; KoPf, M.; Nilges, T.; Zhou, C. Black phosphorus gas sensors. *Acs Nano* **2015**, *9*, 5618–5624. [CrossRef]

30. Wei, Q.; Peng, X. Superior mechanical flexibility of phosphorene and few-layer black phosphorus. *Appl. Phys. Lett.* **2014**, *104*, 372–398. [CrossRef]

31. Yang, G.; Ma, T.; Peng, X. Superior mechanical flexibility and strained-engineered direct-indirect band gap transition of green phosphorene. *Appl. Phys. Lett.* **2018**, *112*, 241904. [CrossRef]

32. Gomes, L.C.; Carvalho, A. Phosphorene analogues: Isoelectronic two-dimensional group-IV monochalcogenides with orthorhombic structure. *Phys. Rev. B* **2015**, *92*, 085406. [CrossRef]

33. Li, Z.Y.; Liu, M.Y.; Huang, Y.; Chen, Q.Y.; Cao, C.; He, Y. Tuning the electronic properties of bilayer group-IV monochalcogenides by stacking order, strain and an electric field: A computational study. *Phys. Chem. Chem. Phys.* **2017**, *20*, 214–220. [CrossRef] [PubMed]

34. Sa, B.; Sun, Z.; Wu, B. The development of two dimensional group IV chalcogenides, blocks for van der Waals heterostructures. *Nanoscale* **2016**, *8*, 1169–1178. [CrossRef]

35. Yang, J.H.; Yuan, Q.; Deng, H.; Wei, S.H.; Yakobson, B.I. Earth-Abundant and Non-Toxic SiX (X = S, Se) Monolayers as Highly Efficient Thermoelectric Materials. *J. Phys. Chem. C* **2017**, *121*, 123–128. [CrossRef]

36. Jiang, H.R.; Zhao, T.S.; Ren, Y.X.; Zhang, R.H.; Wu, M.C. Ab initio prediction and characterization of phosphorene-like SiS and SiSe as anode materials for sodium-ion batteries. *Sci. Bull.* **2017**, *62*, 572–578. [CrossRef]

37. Karmakar, S.; Chowdhury, C.; Datta, A. Two-Dimensional Group IV Monochalcogenides: Anode Materials for Li-Ion Batteries. *J. Phys. Chem. C* **2016**, *120*, 14522–14530. [CrossRef]

38. Mao, Y.L.; Ben, J.; Yuan, J.M.; Zhong, J.X. Tuning the electronic property of two dimensional SiSe monolayer by in-plane strain. *Chem. Phys. Lett.* **2018**, *705*, 12–18. [CrossRef]

39. Perdew, J.P.; Burke, K.; Wang, Y. Generalized gradient approximation for the exchange-correlation hole of a many-electron system. *Phys. Rev. B* **1996**, *54*, 16533–16539. [CrossRef]

40. Ernzerhof, M.; Scuseria, G.E. Assessment of the Perdew–Burke–Ernzerhof exchange-correlation functional. *J. Chem. Phys.* **1999**, *110*, 5029–5036. [CrossRef]

41. Perdew, J.P.; Burke, K.; Ernzerhof, M. Generalized Gradient Approximation Made Simple. *Phys. Rev. Lett.* **1996**, *77*, 3865–3868. [CrossRef] [PubMed]

42. Appalakondaiah, S.; Vaitheeswaran, G.; Lebègue, S.; Christensen, N.E.; Svane, A. Effect of van der Waals interactions on the structural and elastic properties of black phosphorus. *Phys. Rev. B* **2012**, *86*, 035105. [CrossRef]

43. Liu, L.; Yang, Q.; Ye, H.Y.; Chen, X.P.; Zhang, G.Q. Adsorption of gases on monolayer GeSe: A first principle study. In Proceedings of the 18th International Conference on Thermal, Mechanical and Multi-Physics Simulation and Experiments in Microelectronics and Microsystems (EuroSimE), Dresden, Germany, 3–5 April 2017.

44. Ye, H.; Liu, L.; Xu, Y.; Wang, L.; Chen, X.; Zhang, K.; Liu, Y.F.; Koh, S.W.; Zhang, G. SnSe monolayer: A promising candidate of SO2 sensor with high adsorption quantity. *Appl. Surf. Sci.* **2019**, *484*, 33–38. [CrossRef]

45. Rodin, A.S.; Carvalho, A.; Castro Neto, A.H. Strain-Induced Gap Modification in Black Phosphorus. *Phys. Rev. Lett.* **2014**, *112*, 176801. [CrossRef] [PubMed]

46. Nguyen, C.V.; Hieu, N.N. Effect of biaxial strain and external electric field on electronic properties of MoS 2 monolayer: A first-principle study. *Chem. Phys.* **2016**, *468*, 9–14. [CrossRef]

47. Naumis, G.G.; Barraza-Lopez, S.; Oliva-Leyva, M.; Terrones, H. A review of the electronic and optical properties of strained graphene and other similar 2D materials. *Rep. Prog. Phys.* **2017**, *80*, 096501. [CrossRef]

48. Zhang, L.; Tang, Z.K.; Lau, L.; Yin, W.J.; Liu, L.M. Tuning band gaps and optical absorption of BiOCl through doping and strain: Insight form DFT calculations. *Phys. Chem. Chem. Phys.* **2017**, *19*, 20968–20973. [CrossRef]

49. Yu, Z.; Bo, S.; Li, L.; Lei, J. Coupling effects of strain on structural transformation and bandgap engineering in SnS monolayer. *RSC Adv.* **2017**, *7*, 30327–30333.

50. Gao, C.; Zhang, Y.; Yang, H.; Liu, Y.; Liu, Y.; Du, J.; Ye, H.; Zhang, G. A DFT study of In doped Tl2O: A superior NO2 gas sensor with selective adsorption and distinct optical response. *Appl. Surf. Sci.* **2019**, *494*, 162–169. [CrossRef]